ELECTRONIC SUPPLEMENTARY INFORMATION

Small, beautiful and magnetically exotic: $\{V_4W_2\}$- and $\{V_4W_4\}$-type polyoxometalates

M. Rasmussen,[a] C. Näther,[a] J. van Leusen,[b] U. Warzok,[c] C. Schalley,[c] P. Kögerler[b] and W. Bensch[a]

[a] Institut für Anorganische Chemie, Christian-Albrechts-Universität zu Kiel, 24118 Kiel, Germany

[b] Institut für Anorganische Chemie, RWTH Aachen University, 52074 Aachen, Germany

[c] Institut für Chemie und Biochemie der Freien Universität, 14195 Berlin, Germany

Experimental details

Elemental analysis: For CHN elemental analysis an EUROEA Elemental Analyzer (EURO VECTOR Instruments and Software) was used.
IR spectroscopy: IR spectra (400 to 4000 cm^{-1}) were recorded as KBr pellets at room temperature using a Genesis FTIRTM spectrometer from ATI Mattson.
Thermal analysis: DTA-TG investigations were done in a nitrogen atmosphere (purity: 5.0; heating rate 1 K min^{-1}; flow rate: 75 mL min^{-1}; Al_2O_3 crucibles) using a Netzsch STA-409CD instrument.
X-ray powder diffraction: X-ray powder patterns were recorded on a STOE STADI-P diffractometer in transmission geometry (Cu-$K_{\alpha 1}$ radiation, λ = 1.540598 Å; Ge monochromator; flat sample holders, Mythen detector).
UV/Vis/NIR spectroscopy: UV/Vis/NIR spectra (190 – 1100 nm) were employed on an Agilent 8453 spectrophotometer (Agilent Technologies). The deviation amounts to ±0.5 nm with a wavelength reproducibility of ±0.02 nm. For determination of the solubility of compound **2** in water a Carry 5000 instrument was used. The solutions were measured in quartz cuvettes. The absorption at 370 nm was used for determination of the solubility.
Mass spectrometry: Electrospray ionization quadrupole-time-of-flight high resolution mass spectrometric (ESI-Q-TOF-HRMS) experiments were performed with a Synapt G2-S HDMS (Waters Co., Milford, MA, USA) instrument. The flow rate was set to 10 µL min^{-1}, the spray voltage to 2.5 kV, the sample cone voltage to 40 V, the source offset to 80 V, the nebulizer gas to 6 bar and the desolvation gas flow to 500 L h^{-1}. Around these initial settings, the parameters were optimized for maximum abundance of the desired intact cluster ions and minimum abundance of fragments.
Magnetic Measurements: Temperature-dependent susceptibility measurements were performed in the range 2.0–290 K at a magnetic field of 0.1 Tesla using a Quantum Design MPMS-5XL SQUID magnetometer. Field-dependent magnetization measurements in the range 0 – 5 T were performed at 2.0 K. The powdered samples were compacted into cylindrical sample holders (sealed PTFE capsules). The data were corrected for contributions of the sample holder, and the compounds (**1**: $\chi_{m,dia} = -2.82\times10^{-4}$ cm^3 mol^{-1}, **2**: $\chi_{m,dia} = -1.73\times10^{-4}$ cm^3 mol^{-1}).
Single crystal structure analysis: The data for compounds **1** and **2** were collected using an Imaging Plate Diffraction System (IPDS-1) from STOE & CIE using MoK_a radiation. Numerical absorption corrections were performed using X-Red and X-Shape from STOE & CIE. The structures were solved with direct methods using the program SHELXS-97 and the refinements were done against F^2 with SHELXL-97 and SHELXL-2014. All non-hydrogen atoms except one disordered N atom in compound **1** were refined anisotropic. For compound **1** the CH and NH_2 H

atoms were positioned with idealized geometry and were refined using a riding model. The O-H, N-H and terminal NH_2 H atoms were located in difference map, their bond lengths were set to ideal values and afterwards they were refined using a riding model. The terminal N atom of one diene ligand is disordered in two positions and was refined using a split model. For the split position of lower occupancy (sof = 0.2) the H atoms could not be located but were considered in the calculation of the molecular formula. For compound **2** the C-H and NH_2 H atoms were positioned with idealized geometry and refined isotropic using a riding model. The N-H H atoms were located in difference map, their bond lengths were set to ideal values and afterwards they were refined using a riding model. The water O-H H atoms were not located but considered in the calculation of the molecular formula. The positions of two water molecules are only half occupied. Selected crystal data and details of the structure refinements can be found in Table S1. CCDC 1475726 (**1**) and 1475727 (**2**) contain the supplementary crystallographic data for this paper. These data can be obtained free of charge from the Cambridge Crystallographic Data Centre via http://www.ccdc.cam.ac.uk/data_request/cif.

Table S1 Selected data of the data collection and structure refinements of compounds **1** and **2**.

Compound	**1**	**2**
formula	$C_{16}H_{60}N_{12}O_{18}V_4W_2$	$C_{16}H_{64}N_{12}O_{26}V_4W_4$
MW / g·mol^{-1}	1280.22	1779.95
crystal system	triclinic	monoclinic
space group	*P*-1	$P2_1/n$
a / Å	8.4223(7)	13.1608(7)
b / Å	10.4091(8)	12.6983(7)
c / Å	11.8757(10)	27.5889(13)
α	100.76(1)°	90°
β	108.15(1)°	101.30(1)°
γ	100.31(1)°	90°
V / Å^3	940.03(13)	4521.3(4)
T / K	200	180
Z	1	4
D_{calc} / mg·m^3	2.261	2.615
μ / mm^{-1}	7.132	11.015
θ_{max}	28.0°	25.98°
measured refl.	13222	26122
unique refl.	4352	8769
R_{int}	0.0421	0.0530
refl. with $F_0 > 4\sigma(F_0)$	4084	7083
Parameters	240	566
$R_1[F_0 > 4\sigma(F_0)]$	0.0347	0.0359
wR_2 (all refl.)	0.0893	0.0891
GOF	1.024	0.978
$\Delta\rho_{max/min}$ /e·Å^{-3}	1.738 / –2.677	2.013 / –2.368

Table S2 Bond lengths [Å] and angles [°] in compound **1**.

W(1)-O(4)	1.752(3)	V(1)-N(3)	2.176(4)
W(1)-O(5)	1.824(3)	V(1)-N(2)	2.289(4)
W(1)-O(3)	1.894(3)	V(2)-O(7)	1.620(3)
W(1)-V(1)	3.0355(8)	V(2)-O(2)	1.948(3)
W(1)-O(1)	1.910(3)	V(2)-O(5A)	1.981(3)
W(1)-O(2)	2.052(3)	V(2)-N(11)	2.116(4)
W(1)-O(3A)	2.356(3)	V(2)-N(12)	2.152(4)
V(1)-O(6)	1.633(4)	V(2)-O(3)	2.219(3)
V(1)-O(2)	1.924(3)	O(3)-W(1A)	2.356(3)
V(1)-O(1)	1.950(3)	O(5)-V(2A)	1.981(3)
V(1)-N(1)	2.157(4)		

Symmetry transformations used to generate equivalent atoms: A: *–x*+2, *–y*+1, *–z*+2

O(4)-W(1)-O(5)	101.03(15)	O(1)-V(1)-N(2)	87.06(14)
O(4)-W(1)-O(3)	100.49(16)	N(1)-V(1)-N(2)	75.20(15)
O(5)-W(1)-O(3)	99.96(14)	N(3)-V(1)-N(2)	75.39(15)
O(4)-W(1)-O(1)	102.61(16)	O(6)-V(1)-W(1)	106.42(12)
O(5)-W(1)-O(1)	96.56(15)	O(2)-V(1)-W(1)	41.81(9)
O(3)-W(1)-O(1)	148.34(14)	O(1)-V(1)-W(1)	37.69(9)
O(4)-W(1)-O(2)	99.78(15)	N(1)-V(1)-W(1)	126.94(11)
O(5)-W(1)-O(2)	159.06(14)	N(3)-V(1)-W(1)	128.55(13)
O(3)-W(1)-O(2)	78.39(13)	N(2)-V(1)-W(1)	92.18(10)
O(1)-W(1)-O(2)	76.60(13)	O(7)-V(2)-O(2)	104.05(16)
O(4)-W(1)-O(3A)	174.76(14)	O(7)-V(2)-O(5A)	102.15(16)
O(5)-W(1)-O(3A)	76.56(12)	O(2)-V(2)-O(5A)	94.65(14)
O(3)-W(1)-O(3A)	75.54(13)	O(7)-V(2)-N(11)	102.16(18)
O(1)-W(1)-O(3A)	82.36(12)	O(2)-V(2)-N(11)	152.73(15)
O(2)-W(1)-O(3A)	82.88(12)	O(5A)-V(2)-N(11)	87.06(15)
O(4)-W(1)-V(1)	98.60(12)	O(7)-V(2)-N(12)	94.04(17)
O(5)-W(1)-V(1)	134.27(11)	O(2)-V(2)-N(12)	90.37(15)
O(3)-W(1)-V(1)	116.45(9)	O(5A)-V(2)-N(12)	161.30(15)
O(1)-W(1)-V(1)	38.62(10)	N(11)-V(2)-N(12)	80.37(16)
O(2)-W(1)-V(1)	38.70(9)	O(7)-V(2)-O(3)	177.08(16)
O(3A)-W(1)-V(1)	86.30(7)	O(2)-V(2)-O(3)	73.28(12)
O(6)-V(1)-O(2)	107.31(16)	O(5A)-V(2)-O(3)	77.06(12)
O(6)-V(1)-O(1)	106.91(17)	N(11)-V(2)-O(3)	80.65(14)
O(2)-V(1)-O(1)	78.76(13)	N(12)-V(2)-O(3)	87.22(13)
O(6)-V(1)-N(1)	92.26(17)	W(1)-O(1)-V(1)	103.68(15)
O(2)-V(1)-N(1)	159.40(15)	V(1)-O(2)-V(2)	154.64(18)
O(1)-V(1)-N(1)	89.61(14)	V(1)-O(2)-W(1)	99.49(14)
O(6)-V(1)-N(3)	93.25(18)	V(2)-O(2)-W(1)	105.81(14)
O(2)-V(1)-N(3)	87.22(15)	W(1)-O(3)-V(2)	101.48(13)
O(1)-V(1)-N(3)	158.08(16)	W(1)-O(3)-W(1A)	104.46(13)
N(1)-V(1)-N(3)	98.29(17)	V(2)-O(3)-W(1A)	89.92(11)
O(6)-V(1)-N(2)	161.37(16)	W(1)-O(5)-V(2A)	116.35(17)
O(2)-V(1)-N(2)	87.16(14)	N(11)-C(11)	1.486(6)
N(1)-C(1)	1.482(6)	C(11)-C(12)	1.510(8)
C(1)-C(2)	1.504(8)	C(12)-N(12)	1.480(6)
C(2)-N(2)	1.474(6)	N(12)-C(13)	1.476(6)
N(2)-C(3)	1.479(6)	C(13)-C(14)	1.525(7)
C(3)-C(4)	1.528(7)	C(14)-N(13')	1.34(3)

C(4)-N(3)	1.481(6)	C(14)-N(13)	1.430(8)
N(1)-C(1)-C(2)	107.7(4)	N(11)-C(11)-C(12)	108.1(4)
N(2)-C(2)-C(1)	109.5(4)	N(12)-C(12)-C(11)	107.5(4)
C(2)-N(2)-C(3)	113.1(4)	C(13)-N(12)-C(12)	114.6(4)
N(2)-C(3)-C(4)	108.4(4)	N(12)-C(13)-C(14)	115.0(4)
N(3)-C(4)-C(3)	109.3(4)	N(13')-C(14)-N(13)	109.0(15)
N(13)-C(14)-C(13)	107.1(5)		
N(13')-C(14)-C(13)	118.1(14)		

Symmetry transformations used to generate equivalent atoms: A: –*x*+2, –*y*+1, –*z*+2

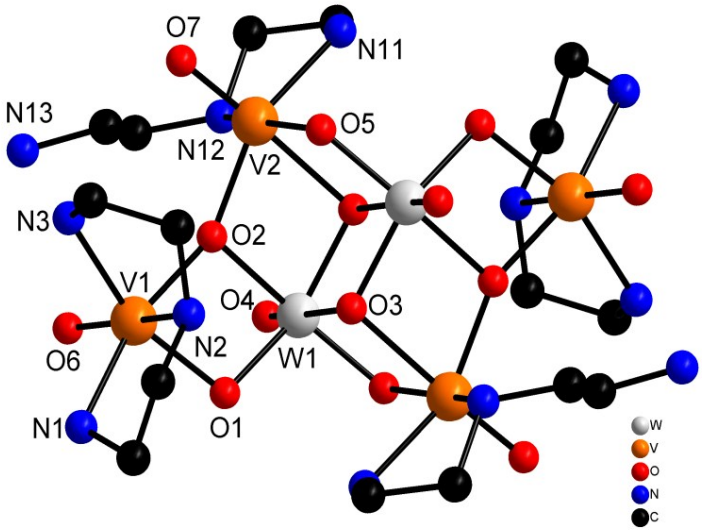

Fig. S1 Numbering scheme of the complex in **1**. Note that H atoms are omitted and only selected atoms are labelled.

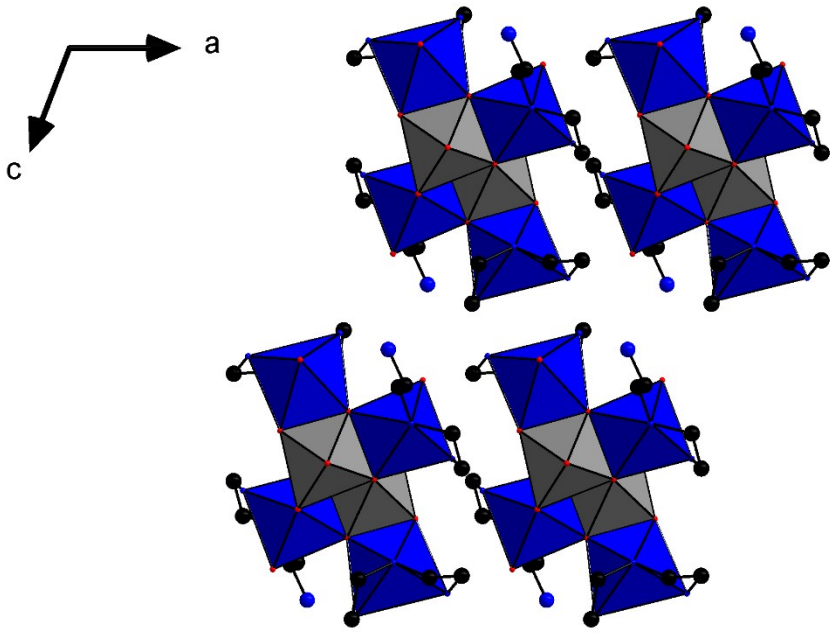

Fig. S2 Arrangement of the {[$V(C_4H_{13}N_3)_4$]W_2O_{14}} clusters in **1** in the (010) plane. H atoms are

omitted for clarity.

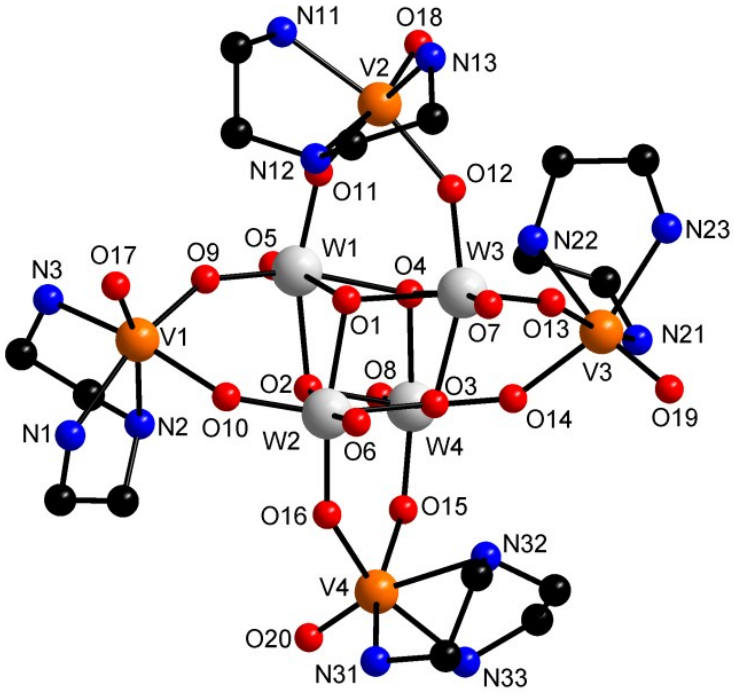

Fig. S3 Numbering scheme of compound **2**. Note that H atoms are omitted and only selected atoms are labelled.

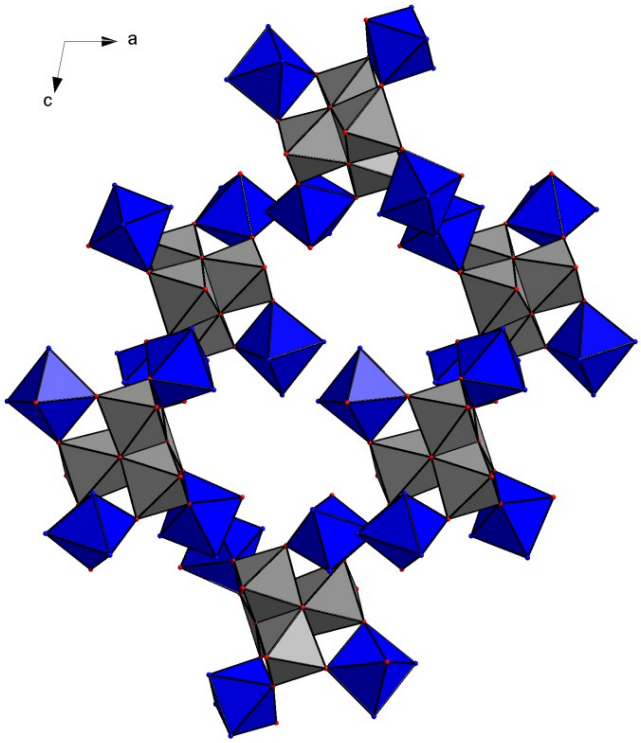

Fig. S4 Arrangement of the molecules in the structure of **2** with view along [010]. C, H, N and O atoms of the ligands and crystal water are omitted for clarity.

Optical spectroscopy

The local symmetry around the two independent V^{4+} ions in **1** is significantly lower than O_h and one can expect that the t_{2g} level is split into three individual levels d_{xy}, d_{xz}, and d_{yz} and the e_g level into $d_{x^2-y^2}$ and d_{z^2}. Hence one can expect up to four electronic transitions between the lowest lying orbital d_{xy} and the four excited states. In the UV/Vis spectrum of **1** (Fig. S5, left) a broad absorption centered around 1.4 eV (11291 cm^{-1}) may be assigned to the electronic transitions between the energetically low-lying states and the second absorption at about 2.06 eV (16695 cm^{-1}) is caused by transitions to the two most excited states. Because the two independent V^{4+} ions are in different chemical environments the electronic transitions may energetically differ but individual absorptions are hidden under the broad peaks. The remaining transitions are not observed in the spectrum and they may be covered by the broad charge transfer band which sets in at about 2.6 eV (20800 cm^{-1}). For compound **2** the first absorption has a maximum at 1.49 eV (12017 cm^{-1}) (Fig. S5, right) which can be assigned in the same way as for **1**. The peak is less smeared out than in **1** due to the identical environments of the V^{IV} centers. The maximum of the second absorption is shifted to 2.24 eV (18066 cm^{-1}) compared to that observed for **1** may be caused by differing V-N/O interactions leading to a different splitting of the energy levels. Like for **1** the remaining transitions are hidden under the broad charge transfer band.

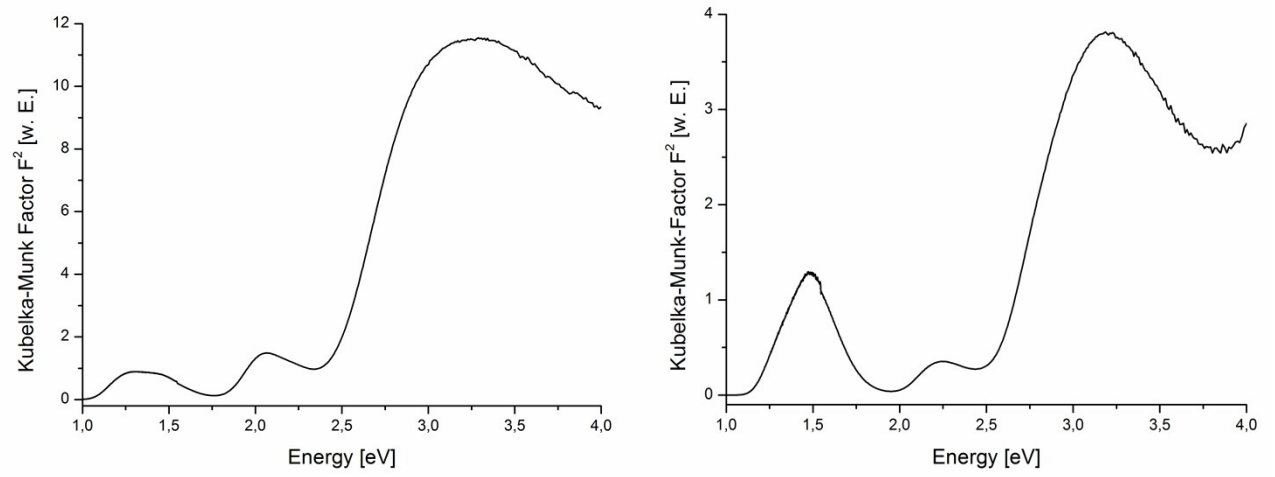

Fig. S5 UV/Vis spectra of compound **1** (left) and **2** (right).

The IR spectra of the two compounds are displayed in Fig. S6. The region above 2000 cm^{-1} shows absorptions of H_2O (ν(OH) stretch, ca. 3400 cm^{-1}), the stretching vibrations of NH_2/NH between 3150 and 3340 cm^{-1} and CH_2 stretching modes around 2900 cm^{-1}. The NH_2 deformation band is located at about 1590 cm^{-1} and several further absorptions of CH_2/NH_2 as well as C-C/C-N modes are located between 1000 and 1450 cm^{-1}. The M-O and M-O-M/M' based signals are located below 1000 cm^{-1} for both tungsten and vanadium. A simple assignment of the absorptions is not straightforward because the different absorptions strongly overlap. The intense V^{IV}=O stretching vibration in fivefold coordinated complexes is observed between about 930 and 1000 cm^{-1} depending on the coordination environment of the V(IV) center. The energetic position of the absorption in such complexes depends on the degree of oxygen to donate and of vanadium to accept electron density. While the presence of ligands around the V(IV) center likely does not significantly affect the donating tendency of the oxygen atom, the electron density-accepting ability

of V(IV) is significantly influenced by the co-ligands, where an increase in electron density in the V 3d orbitals is expected to cause a bathochromic shift for the V=O stretching mode. For V(IV) center in a six-fold coordination environment the V=O stretching vibration may occur at lower wavenumbers. For compound **1** the absorption located at 940 cm^{-1} is most probable the V=O stretch, while a shift to 920 cm^{-1} is observed for **2**. The M-O-M modes are below about 900 cm^{-1} and depend on the connectivity. In **1** four types of oxygen atoms are present: terminal, μ_2 (connecting 1 V and 1 W); μ_3 (connecting one V and two W), and μ_3 (connecting 2 V and 1 W); in **2** only three types are observed: terminal, μ_2 (connecting 1 V and 1 W), and μ_3 (connecting 3 W). The differing connection schemes may explain the presence of two well-separated absorptions for **1** (824 and 764 cm^{-1}) and only one band (788 cm^{-1}) for **2**.

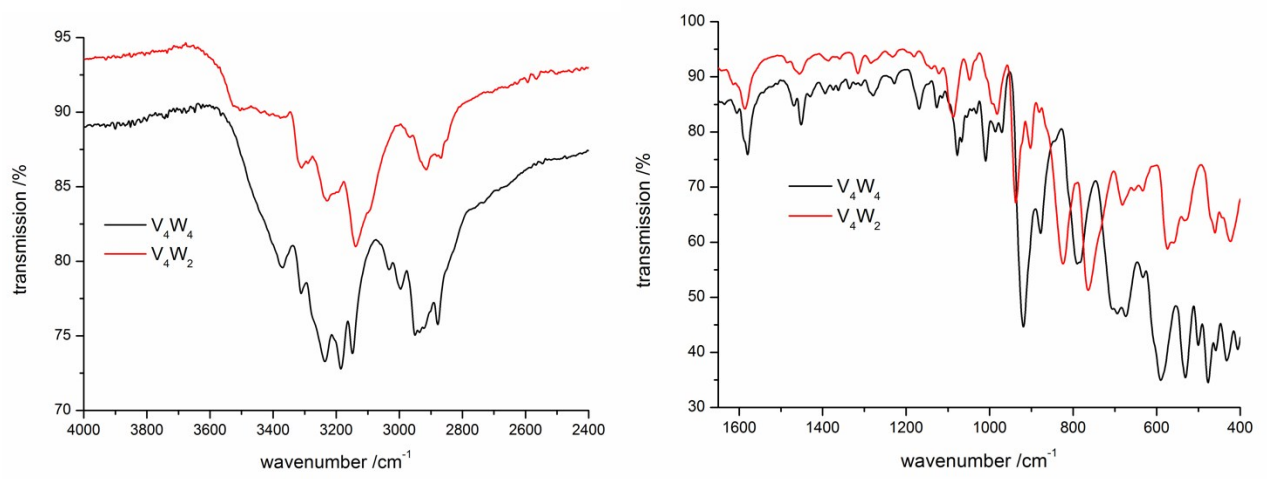

Fig. S6 The IR spectra (KBr pellets) of compounds **1** (red) and **2** (black).

Thermal stability

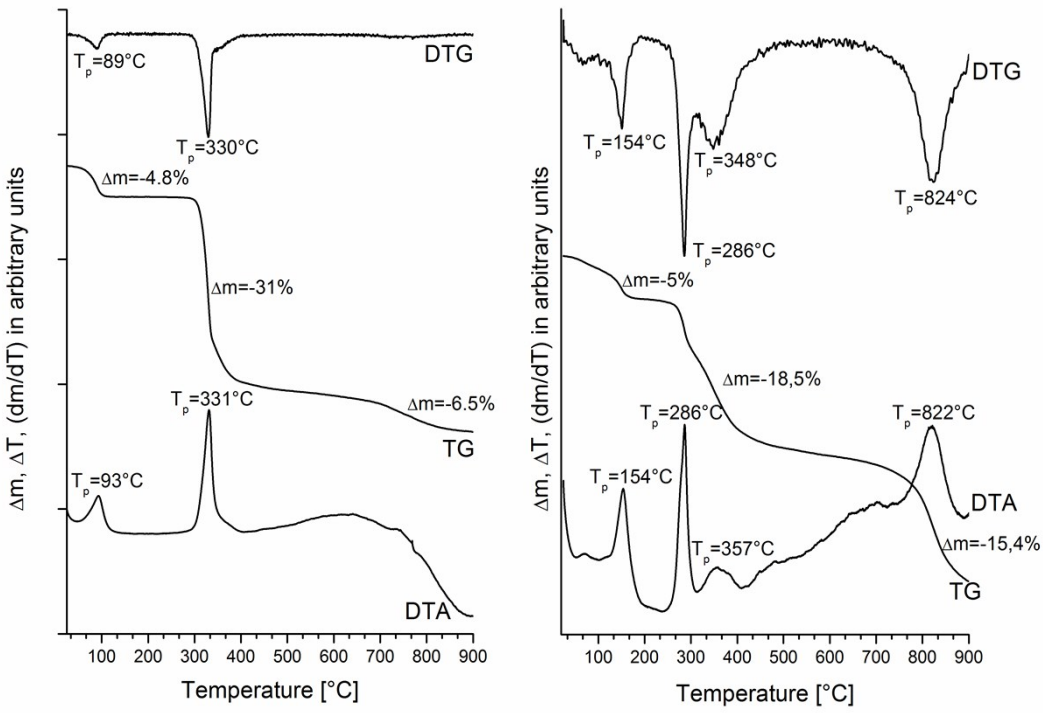

Fig. S7 DTA-TG and DTG curves of the thermal decomposition of **1** (left) and **2** (right).

Both compounds release water (Fig. S7) during heating in a first decomposition step accompanied by an exothermic event in the DTA trace. The dehydrated samples are remarkable stable and the plateau in the TG curve for **1** extends up to about 300 °C and to ca. 260 °C for **2**. The weight losses of 4.8 respectively 5% are in perfect agreement with the number of crystal water molecules. Heating the compounds up to 900 °C, several thermal events are observed leading to decomposition of the pristine materials. In further experiments the thermal decomposition was stopped at 200 °C and X-ray powder patterns of the residues were recorded. Upon heating, no drastic changes between the XRD patterns are observed (Fig. S8), indicating that the emission of water only slightly changes the arrangements of the cluster molecules. The crystallinity of sample **1** seems to be not significantly affected, while that of compound **2** is slightly affected.

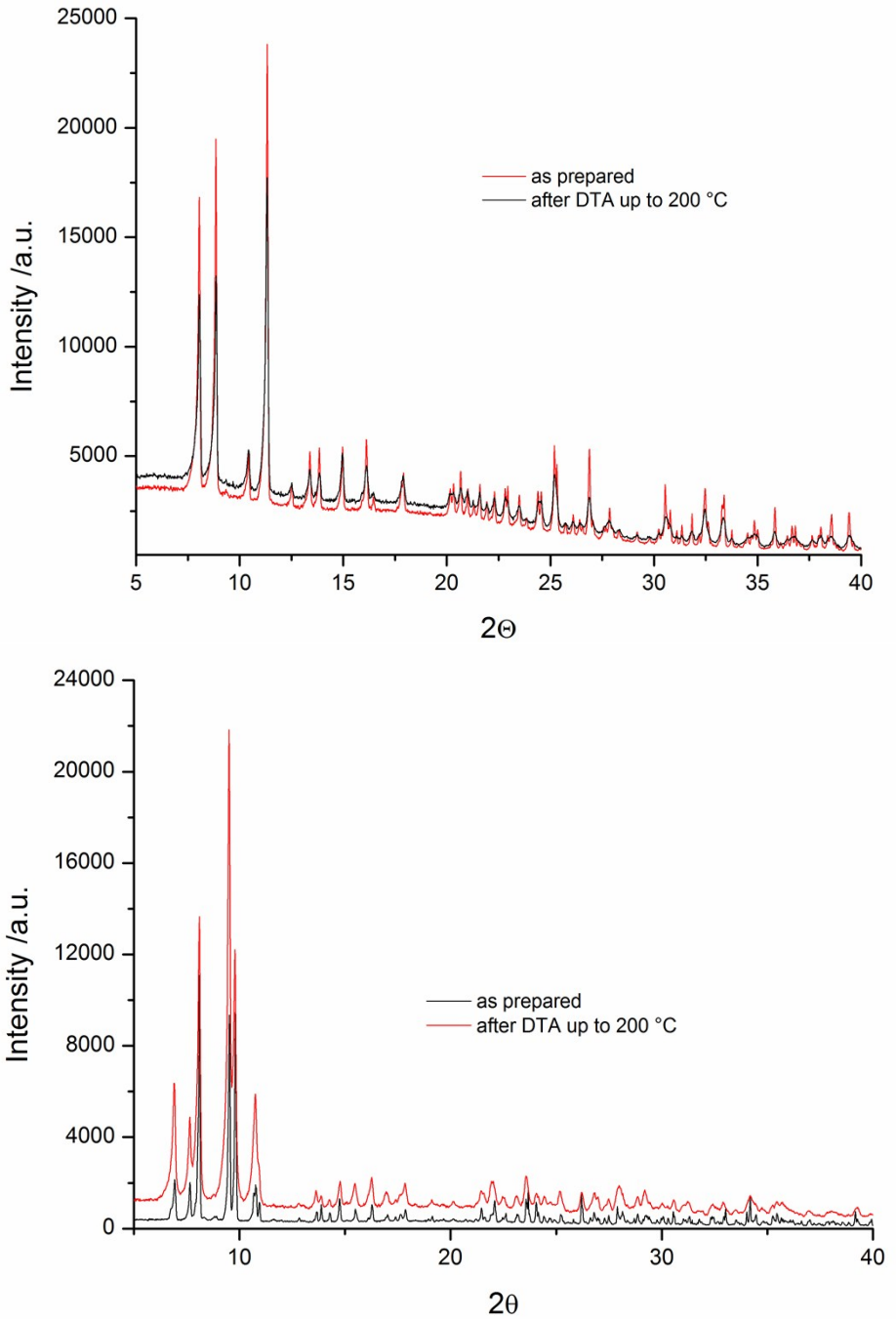

Fig. S8 X-ray powder patterns of compounds **1** (top) and **2** (bottom) recorded before and after the DTA-TG experiments.